# 1 Plasminogen Activator Inhibitor-1 promotes aortic aging-

# 2 like pathophysiology in humans and mice

- 3 Alireza Khoddam<sup>1\*</sup>, Anthony Kalousdian<sup>1\*</sup>, Mesut Eren<sup>1</sup>, Saul Soberanes<sup>1</sup>, Andrew Decker<sup>1</sup>,
- 4 Elizabeth J. Lux<sup>1</sup>, Benjamin W. Zywicki<sup>1</sup>, Brian Dinh<sup>1</sup>, Bedirhan Boztepe<sup>2</sup>, Baljash S. Cheema<sup>2</sup>,
- 5 Carla M. Cuda<sup>2</sup>, Hiam Abdala-Valencia<sup>2</sup>, Arun Sivakumar<sup>2</sup>, Toshio Miyata<sup>3</sup>, Lisa D. Wilsbacher<sup>1,2</sup>¶
- 6 & Douglas E. Vaughan<sup>1,2</sup>¶

7

- <sup>1</sup>Feinberg Cardiovascular and Renal Research Institute, <sup>2</sup>Department of Medicine, Northwestern
- 9 University Feinberg School of Medicine, Chicago, IL, USA
- 10 <sup>3</sup>Tohoku University Graduate School of Medicine, Sendai, Japan

11

- 12 \* A. Khoddam and A. Kalousdian are co-first authors.
- 13 ¶ LDW and DEV and co-corresponding and co-senior authors.

14

- 15 Corresponding authors:
- 16 Lisa D. Wilsbacher
- 17 Northwestern University Feinberg School of Medicine
- 18 Simpson Querrey Biomedical Research Center 8-404
- 19 303 E. Superior St.
- 20 Chicago, IL 60611
- 21 Fax: 312-503-0662
- 22 Telephone: 312-503-6880
- 23 Email: lisa.wilsbacher@northwestern.edu
- 24 Douglas E. Vaughan
- 25 Northwestern University Feinberg School of Medicine
- 26 Simpson Querrey Biomedical Research Center 8-516
- 27 303 E. Superior St.
- 28 Chicago, IL 60611
- 29 Fax: 312-618-7365
- 30 Telephone: 312-503-1531
- 31 Email: d-vaughan@northwestern.edu

- 33 Conflict of interest: Toshio Miyata is founder and Chairman of Renascience; Renascience which
- 34 did not influence experimental design or data interpretation. All other authors report no competing
- 35 interests.

## Abstract

36

37

38

39

40

41

42

43

44

45

46

47

48

49

50

51

52

53

54

Plasminogen activator inhibitor-1 (PAI-1), encoded by SERPINE1, contributes to age-related cardiovascular diseases (CVD) and other aging-related pathologies. Humans with a heterozygous loss-of-function SERPINE1 variant exhibit protection against aging and cardiometabolic dysfunction. We engineered a mouse model mimicking the human mutation (Serpine1<sup>TA700/+</sup>) and compared cardiovascular responses with wild-type littermates. Serpine 1<sup>TA700/+</sup> mice lived 20% longer than littermate controls. Under L-NG-Nitro-arginine methyl ester (L-NAME)-induced vascular stress, Serpine 1<sup>TA700/+</sup> mice exhibited diminished pulse wave velocity (PWV), lower systolic hypertension (SBP), and preserved left ventricular diastolic function compared to controls. Conversely, PAI-1-overexpressing mice exhibited measurements indicating accelerated cardiovascular aging. Single cell transcriptomics of Serpine1<sup>TA700/+</sup> aortas revealed a vascularprotective mechanism with downregulation of extracellular matrix regulators Ccn1 and Itab1. Serpine 1<sup>TA700/+</sup> aortas were also enriched in a cluster of smooth muscle cells that exhibited plasticity. Finally, PAI-1 pharmacological inhibition normalized SBP and reversed L-NAMEinduced PWV elevation. These findings demonstrate that PAI-1 reduction protects against cardiovascular aging-related phenotypes, while PAI-1 excess promotes vascular pathological changes. Taken together, PAI-1 inhibition represents a promising strategy to mitigate age-related CVD.

Key Words: Plasminogen Activator Inhibitor-1, Cardiovascular Aging, Vascular Stiffness

## Introduction

Plasminogen activator inhibitor-1 (PAI-1) is a critical contributor in age-related cardiovascular diseases (CVD) (1, 2). PAI-1 was originally identified as an inhibitor of tissue-type plasminogen activator (t-PA) and urokinase plasminogen activator (u-PA), and therefore it promotes vascular thrombosis (3). However, subsequent studies revealed that PAI-1 also contributes to senescence: senescent cells secrete higher PAI-1 levels as part of the Senescence Associated Secretory Phenotype (SASP), accelerating the accumulation of additional senescent cells (4); furthermore, PAI-1 is also a necessary and sufficient mediator of senescence (4–6). Additional work in mice demonstrated that PAI-1 also impacts aging (7). Clinically, elevated PAI-1 levels in humans correlate with coronary disease (8, 9), increased vascular stiffness (10), obesity (11, 12), and diabetes (13). Methylation-based prediction of PAI-1 expression levels consistently predict earlier time-to-mortality (14). Experimental studies link PAI-1 to arteriosclerosis (15), age-dependent coronary thrombosis (16, 17), endothelial dysfunction (18), and disruptions in lipid metabolism (19). These findings suggest PAI-1 as a potential target for combating age-related cardiovascular decline.

Pharmacological inhibition of PAI-1 has gained momentum due to its pleotropic role in age-related diseases (20). Small molecule inhibitors have been developed to reduce PAI-1 activity, with evidence in animal models showing improvements in vascular function (21), reduced thrombosis (22), and amelioration of metabolic dysfunction (23). In humans, a rare dinucleotide duplication mutation in the *SERPINE1* gene (designated SERPINE1c.699\_700dupTA) was identified as a founder mutation in a Swiss Amish population in Berne, Indiana. This loss of function (LOF) mutation leads to a dose-dependent reduction in plasma PAI-1 levels (both activity and antigen) (24). Individuals with LOF heterozygosity exhibit longer leukocyte telomere lengths, lower fasting

insulin, and reduced diabetes prevalence (25). This "heterozygous advantage" is also characterized by extending the human lifespan by a median of 10 years (25).

81

82

83

84

85

86

87

88

89

90

91

92

93

94

95

96

97

79

80

The risk of cardiovascular disease increases with age (26, 27), and this risk culminates with cardiovascular disease as the leading cause of death worldwide (28). Vascular stiffness accelerates CVD development, especially in aging populations, by damaging the microvasculature of organs like the brain and kidneys; elevated vascular stiffness increases the risk of hypertension, atherosclerosis, heart attacks, cognitive decline, and strokes (29). Arterial stiffness, measured physiologically by pulse wave velocity (PWV), is well-established to rise with age (30-34); notably, increases in PWV precede overt hypertension and cardiovascular disease (31–33), and PWV has been described as a tool to measure vascular aging (31). Recent work suggested that vascular aging is one of the primary drivers of systemic aging (35) and a major contributor to the development of various other age-related diseases. Cellularly, endothelial cells regulate vascular tone and vasodilation via nitric oxide (NO) production by endothelial NO synthase (eNOS) (36). Aging in murine models has been linked to increased uncoupling of the eNOS complex (37), and PAI-1 was recently identified as a negative regulator of eNOS, impairing NO production in vitro (18). This in vitro finding partly explains the cardiovascular and longevity benefits of PAI-1 reduction. Thus, we hypothesize that reducing circulating PAI-1 levels protects against vascular stiffness and vascular aging.

98

99

100

101

102

103

104

In this report, we investigated the role of PAI-1 on cardiovascular physiology using genetically engineered mouse models. We reverse engineered a mouse line carrying a dinucleotide duplication mutation in *Serpine1* exon 4 (*Serpine1*<sup>c.699</sup>\_700dupTA), mirroring the human LOF mutation associated with protection against biological aging. We subsequently treated heterozygous mutated mice (hereafter referred to as *Serpine1*<sup>TA700/+</sup>) with an eNOS inhibitor to model aging-related vascular stiffening and increased PWV. Additionally, we used another mouse model

overexpressing stabilized human PAI-1 (16) to compare PWV changes with aging. Bulk and single-cell RNA sequencing identified candidate genes associated with PAI-1 reduction's protective effects. Lastly, we tested the ability of a small molecule PAI-1 inhibitor to reverse damages to the vasculature via eNOS inhibition.

### Results

105

106

107

108

109

110

111

112

113

114

115

116

117

118

119

120

121

122

123

124

125

126

127

128

#### Heterozygous SERPINE1 Deficiency Confers Vascular Fitness in Humans

To build on the initial findings in the Swiss Amish population in Berne, IN, (25) we recruited additional individuals from this population and expanded the phenotyping protocol to include PWV. We compared individuals carrying the SERPINE1 c.699 700dupTA mutation (SERPINE1TA700/+, n=33 with 11 males and 22 females) to sex and age-matched unaffected controls (SERPINE1+/+, n=33 with 11 males and 22 females). When adjusting for age and sex, we found that PWV values were significantly lower in the SERPINE1<sup>TA700/+</sup> group, suggesting a potential protective effect against vascular stiffening (Table 1). The parameter estimate for genotype was 1.182 m/s (95% CI: -1.784 to - 0.580, P = 0.0002), indicating that, after adjusting for age and sex, SERPINE1<sup>TA700/+</sup> carriers had PWV values that were on average 1.182 m/s lower than non-carriers. Based on clinical observations, this magnitude of reduction is linked to a meaningful decrease in all-cause mortality risk (38). Using the same data from this cohort, we performed simple linear regression and found a positive correlation between age and PWV. The slope of each line did not differ between genotypes; however, elevation of the line was lower in SERPINE1<sup>TA700/+</sup> carriers as compared to SERPINE1<sup>+/+</sup> individuals, as expected from our adjusted analyses (Figure 1A). We also analyzed the aggregated PWV averages of individuals and found that PWV is roughly 12% lower in SERPINE1<sup>TA700/+</sup> carriers compared to noncarriers (Figure 1B). Together, these statistical analyses confirm that PWV increases with age in both genotypes at a comparable rate; however, the SERPINE1<sup>TA700/+</sup> variant is associated with an overall lower PWV,

even after adjusting for age. Stratifying the PWV values by biological sex yielded consistent results, with statistically significant differences observed in both males and females (Supplemental Figure 1). Our findings prompted us to dissect the mechanisms underlying this vascular improvement using experimental animal models.

### Serpine1<sup>TA700/+</sup> Mice Exhibit Longer Lifespan and Reduced Aging-Related Aortic

#### **Stiffness**

To examine potential mechanisms by which the LOF *SERPINE1*<sup>c.699</sup>\_700dupTA mutation confers protection against biological aging (25), we utilized CRISPR-based gene editing on C57BL6/J mice to insert a TA dinucleotide at the end of exon 4 of *Serpine1* gene (Figure 1C and Supplemental Figure 2). We measured PAI-1 levels in circulating plasma from mutated mice using ELISA. *Serpine1*<sup>TA700/+</sup> and *Serpine1*<sup>TA700/TA700</sup> exhibited a 50% and 100% reduction, respectively, in circulating PAI-1 antigen levels compared to *Serpine1*<sup>+/+</sup> controls (Figure 1D). We measured PWV of *Serpine1*<sup>TA700/+</sup> and control mice older than 85 weeks. We found that *Serpine1*<sup>TA700/+</sup> mice exhibit roughly 20% lower PWV compared to *Serpine1*<sup>+/+</sup> mice (Figure 1E). Akin to the longer lifespan phenotype observed in humans (25), *Serpine1*<sup>TA700/+</sup> exhibited a 20% longer overall survival compared to wild-type littermates (Figure 1F). The length of lifespan is not sex-dependent between male and female *Serpine1*<sup>TA700/+</sup> mice (Supplemental Figure 3).

## Serpine1 Haploinsufficiency Protects Against L-NAME-induced Aging-Like

### **Pathophysiology**

We hypothesized that the reduction of PAI-1 in *Serpine1*<sup>TA700/+</sup> would protect the mice against cardiovascular stress. To model hypertension associated with aging, we treated *Serpine1*<sup>TA700/+</sup> mice and control littermates with L-NAME (Figure 2A). This established model inhibits eNOS, causing endothelial dysfunction (39), increased senescence (21), arterial stiffness (40), and hypertension (41). We quantified changes associated with L-NAME-induced stress using

physiological measures, including descending aorta PWV, systolic blood pressure (SBP), and diastolic function (E/e'). At baseline, PWV, SBP, and E/e' were comparable between Serpine1<sup>TA700/+</sup> mice and control littermates (Figure 2, B-D). Following 8 weeks of L-NAME treatment, we found that the increase in PWV, SBP, and E/e' were significantly attenuated in Serpine1<sup>TA700/+</sup> mice compared to control littermates (Figure 2, B-D). Stratifying measurements by biological sex confirmed consistent and statistically significant differences across groups, with only the end-of-study SBP in male Serpine1<sup>TA700/+</sup> mice not reaching statistical significance (Supplemental Figure 4). Furthermore, the increase in PWV with an 8 week-L-NAME treatment in 3-month-old mice for both Serpine1<sup>+/+</sup> and Serpine1<sup>TA700/+</sup> animals was comparable to PWV values of aged mice (Supplemental Figure 5); this observation provides evidence that L-NAME treatment recapitulates aging-like vascular pathologies associated with chronological aging as measured using PWV. These data suggest that PAI-1 is necessary to promote the aging-like pathophysiological changes induced by L-NAME.

### **PAI-1 Overexpression Exacerbates Aging-Like Pathophysiology**

Given our results in mice with genetic reduction in PAI-1, we hypothesized that overexpression of PAI-1 would heighten the adverse increases in vascular physiology measures that we observed in L-NAME treated mice. To test this hypothesis, we utilized a mouse model that expresses a stabilized form of human PAI-1 under the murine preproendothelin-1 promoter, maintained on a B6.D2 background (hereafter referred to as *SERPINE1*StabOE) (16). *SERPINE1*StabOE mice and wild-type littermate controls underwent baseline physiological studies at 12 weeks of age and reassessment at 24 weeks of age (end of study) (Figure 3A). At baseline, *SERPINE1*StabOE mice showed elevated SBP and E/e' compared to littermate controls (Figure 3, C and D), indicating that excess PAI-1 can increase these measures as early as 12 weeks of age. We reassessed the same mice after 12 weeks of aging alone and found further increases in PWV, SBP, and E/e' in *SERPINE1*StabOE mice compared to control mice (Figure 3, B-D). Stratifying measurements by

biological sex confirmed consistent and statistically significant differences all across groups (Supplemental Figure 6). The physiologic observations suggest that excess PAI-1 expression is sufficient to drive an increase in aging-like pathophysiological changes by 12 weeks of age with progressive worsening in vascular stiffening or vascular tone at 24 weeks of age.

### Bulk RNA sequencing Identifies Ccn1 as a Differentially Expressed gene in

#### Serpine1<sup>TA700/+</sup> Aortas Exposed to L-NAME

Building on our physiological findings, we investigated specific pathways that may mediate the protection observed in *Serpine1*<sup>TA700/+</sup> following L-NAME. We first performed bulk RNA sequencing on the aortas of *Serpine1*<sup>TA700/+</sup> and control littermates following 8 weeks of L-NAME (Figure 4A). *Serpine1* was among the most significantly reduced differentially expressed genes in *Serpine1*<sup>TA700/+</sup> aortas, consistent with the genetic reduction of *Serpine1* in this model. RNA sequencing also revealed significantly reduced expression of *Ccn1* in *Serpine1*<sup>TA700/+</sup> aortas compared to controls after 8 weeks of L-NAME treatment (Figure 4B). We then used immunofluorescence to visualize differences in CCN1 protein (Figure 4, C-E) and found that *Serpine1*<sup>TA700/+</sup> aortas exhibit reduced CCN1 protein. This data highlights effects of PAI-1 reduction on *Ccn1* expression and CCN1 protein.

#### Aorta scRNA-seq Differences in Serpine1<sup>TA700/+</sup> Mice Exposed to L-NAME

To gain deeper insights into the cellular mechanisms underlying the observed transcriptional changes, we performed single-cell RNA sequencing (scRNA-seq) on independent aorta samples using the same study design as bulk RNA sequencing (Figure 4A). This approach allowed us to dissect the cellular composition and gene expression dynamics driving the vascular phenotype. We sequenced 29,535 cells from the aortas of 4 *Serpine1*<sup>TA700/+</sup> and 6 control mice (Figure 5A). The *Serpine1*<sup>TA700/+</sup> and control aortas yielded 12,001 and 17,534 cells, respectively (Figure 5B). More than 60% of the sequenced cells were identified as vascular smooth muscle cells (SMCs),

while endothelial cells (ECs) accounted for just over 2%. According to previous literature on SMCs (42, 43), we used gene markers Tnfrsf11b, Lgal3, and Acan to identify chondrocyte-like SMCs that resemble chondrocytes (Supplemental Figure 7A). We also defined ECM-Secretory SMC as cells with moderate expression of contractile markers such as Myh11 and Mylk (but low Acta2 expression (44)), as well as high expression of extracellular matrix protein genes such as Vcan that have been associated with "young" ECM (45, 46) (Supplemental Figure 7B). Utilizing KEGG pathway enrichment, we found that cells from Serpine 1<sup>TA700/+</sup> aortas are enriched for pathways critical for vascular aging such as longevity regulation, autophagy (47), and FoxO signaling (48) (Figure 5C). When examining specific genes in our dataset, we observed that aortic Serpine1 expression in Serpine 1<sup>TA700/+</sup> mice was lower when compared to control (Figure 5, D-G). We found the largest difference in Serpine1 transcripts in SMC clusters while fibroblasts and ECs exhibited little difference (Figure 5, D-G and Supplemental Figure 7C). Consistent with our bulk RNA seq results, we found reduced aortic *Ccn1* expression in *Serpine1*<sup>TA700/+</sup> compared to control cells (Figure 5, H-K). CCN1 protein (also known as CYR61 (49)) has been shown to interact with Integrin β1 (ITGB1) to promote senescence (50–52), a hallmark of cardiovascular aging (53). Interestingly, our scRNA-seq data analysis revealed reduced expression of the gene encoding Integrin β1, Itab1, in Serpine1<sup>TA700/+</sup> aortas compared to controls (Figure 5, L-O). The greatest difference in Ccn1 and Itgb1 expression between the two genotypes was observed in SMC clusters (Figure 5, J and N and Supplemental Figure 7, D and E). This finding suggests that reduced *Itab1* expression in Serpine1<sup>TA700/+</sup> may attenuate ITGB1 signaling, further limiting the pro-senescent effects of CCN1 and contributing to vascular protection. To further investigate the dynamics of cell state transitions within the SMC lineage, we performed steady state RNA velocity (54) and CellRank (55) analyses on the scRNA-seq data (Figure 6). In Serpine 1+/+ aortas, RNA velocity vectors followed consistent trajectories within SMC subclusters towards mature SMCs, suggesting limited transition to alternative fates (Figure 6A). In contrast,

202

203

204

205

206

207

208

209

210

211

212

213

214

215

216

217

218

219

220

221

222

223

224

225

226

Serpine 1<sup>TA700/+</sup> aortas displayed more diverse velocity patterns, suggesting increased transcriptional plasticity (Figure 6B). Notably, SMCs in *Serpine* 1<sup>TA700/+</sup> mice exhibited trajectories toward ECM-secretory SMCs and fibroblasts, whereas SMCs and fibroblasts in control aortas remained confined to their cluster (Figure 6, C and D). CellRank further supported these findings by predicting that ECM-secretory SMCs in *Serpine* 1<sup>+/+</sup> aortas could transition back to other SMC states (Figure 6F). In *Serpine* 1<sup>TA700/+</sup> aortas, these ECM-secretory SMCs demonstrated enhanced potential to transition to mature SMCs (Figure 6E). These findings suggest that PAI-1 reduction enhances the flexibility of SMC cell states, potentially promoting adaptive remodeling and limiting the terminal differentiation programs associated with vascular aging and pathology.

#### Pharmacological PAI-1 Inhibition Reverses L-NAME-Induced Increase in Pulse

#### Wave Velocity

Lastly, we investigated whether pharmacological PAI-1 inhibition can attenuate L-NAME-induced vascular pathophysiology. We administered L-NAME to 20-week-old *Serpine1*\*/\* mice for 4 weeks, followed by 6 weeks of combined L-NAME and PAI-1 inhibitor TM5614 treatment or control chow; during these treatments, we monitored changes in PWV at baseline, after L-NAME exposure, and after the combined treatment (Figure 7A). Consistent with prior results, L-NAME treatment led to significant increases in PWV, SBP, and DBP (Figure 7, B-D). Remarkably, TM5614 administration at week 4 restored PWV to baseline levels at 10 weeks despite ongoing L-NAME treatment (Figure 7B). Additionally, we found that the subsequent TM5614 co-treatment significantly reduced the L-NAME-induced increase in systolic (Figure 7C) and diastolic blood pressure (Figure 7D). In contrast, the mice given control chow exhibited high PWV, SBP, and DBP comparable to 4-week measurements. Stratifying measurements by biological sex confirmed consistent and statistically significant differences all across groups (Supplemental Figure 8). These findings imply that PAI-1 inhibition can decrease and even reverse pre-existing aging-related cardiovascular pathophysiology.

## Discussion

253

254

255

256

257

258

259

260

261

262

263

264

265

266

267

268

269

270

271

272

273

274

275

276

277

We previously demonstrated that a rare loss-of-function variant in the human SERPINE1 gene is associated with protection against various aspects of biological aging (25). This study extends those findings by characterizing additional members of the Amish community with the mutation and providing additional evidence for the "heterozygous advantage" model. In this model, low to moderate levels of PAI-1 protect organisms from aging, while complete PAI-1 deficiency leads to cardiac fibrosis (56, 57), and excess PAI-1 drives accelerated aging (5, 7). Individuals who are homozygous for the SERPINE1 loss-of-function mutation develop mesocardial and subepicardial cardiac fibrosis through TGFβ signaling (56, 57). Similarly, Serpine 1-/- mice develop agedependent infiltrative cardiac fibrosis (58, 59). However, detailed protective mechanisms of the heterozygous advantage remain challenging to define in human populations. To address this barrier and further investigate physiologic and molecular roles for PAI-1 in vascular aging, we generated a mouse model (Serpine 1<sup>TA700/+</sup>) that faithfully recapitulates the human mutation. Here, we show that Serpine1TA700/+ mice were protected from L-NAME-induced cardiovascular pathophysiology, which indicates that elevated PAI-1 activity is necessary for vascular aging. While the L-NAME model is not a perfect representation of vascular aging, and its effects on neuronal nitric oxide synthase and central regulation are not fully accounted for, we show that the resulting phenotype of elevated PWV closely resembles that observed during natural aging (Figure 1F). We also used transgenic overexpression of PAI-1 (SERPINE1StabOE) to show that a significant excess of PAI-1 is sufficient to drive premature vascular aging. Lastly, and most clinically relevant, we found that the oral PAI-1 inhibitor TM5614 was able to reverse L-NAMEinduced cardiovascular pathophysiology. These findings provide a substantial contribution to the already compelling evidence that plasma PAI-1 is an important clinical predictor of vascular stiffness, hypertension and diastolic dysfunction, especially in individuals with obesity and diabetes. Given the rarity of loss-of-function

mutations in SERPINE1, it is likely that the 43% of the world population with visceral obesity (2.5 billion people over age 18) (60) have a durable and consequential systemic excess of PAI-1, as BMI is the dominant determinant of plasma PAI-1 levels (61). Understanding the molecular mechanisms underlying PAI-1 reduction will rapidly translate into reducing age-related CV disease for billions of people worldwide. At the molecular level, we identified Ccn1 and Itab1 as candidate genes potentially mediating the downstream effects of PAI-1. These observations raise important questions about the mechanisms through which PAI-1 influences the expression of these genes. Prior studies have implicated *Ccn1* in pathological vascular remodeling (62), fibrosis (63), and atherosclerosis (64). Moreover, CCN1 (50) utilizes integrin β1 to induce downstream signaling; and interestingly, the gene encoding for integrin b1 (Itab1) was also downregulated in Serpine1<sup>TA700/+</sup> mice. We hypothesize that the suppression of the Ccn1 and Itqb1 axis by PAI-1 reduction may serve as a protective mechanism. The elevated expression of these genes in the presence of high PAI-1 levels underscores the need for further investigation into how PAI-1 modulates their transcription and their downstream signaling pathways. Although ECs lining the vasculature have been considered primary contributors of PAI-1 to the bloodstream in pathological conditions (65, 66), scRNA-seq showed that Serpine1 expression is more prominent in SMCs of the aorta than in ECs; our results are in keeping with a recent study of calcineurin-mediated hypertension and abdominal aortic aneurysm in mice (67). Additionally, steady state RNA velocity analysis suggested that SMCs from Serpine1<sup>TA700/+</sup> mice are more likely to adopt an ECM-Secretory SMCs phenotype with low-to-moderate expression of contractile genes and high expression of ECM genes (Figure 6). CellRank analysis further suggested that SMCs from Serpine 1+++ mice adopt a mature SMC phenotype with minimal plasticity, while SMCs from Serpine 1<sup>TA700/+</sup> mice display higher plasticity and higher likelihood to adopt the ECM-Secretory phenotype after L-NAME exposure. ECM genes with high levels of expression in the ECM-Secretory SMC population include Lama2 and Vcan. These genes have

278

279

280

281

282

283

284

285

286

287

288

289

290

291

292

293

294

295

296

297

298

299

300

301

302

304 been implicated in the maintenance of healthy, "young" ECM in other tissues. Mutations in LAMA2 305 cause forms of muscular dystrophy due to weak interstitial connections between striated muscle 306 cells (68). In neonatal myocardium, Vcan was identified as a pro-proliferative proteoglycan 307 supporting cardiomyocyte proliferation (45, 46). Additional studies are needed to further 308 investigate this population of SMCs, their role in maintaining a "young" ECM that maintains pliant 309 vasculature, and how excess PAI-1 promotes the transition toward SMC populations that reduce 310 vascular compliance. 311 Remarkably, TM5614 administration ameliorated cardiovascular pathophysiology observed in 312 wild-type mice subjected to L-NAME. These results align with earlier studies demonstrating the 313 therapeutic potential of PAI-1 inhibitors in mitigating metabolic dysfunction (19, 23, 69, 70). 314 fibrosis (21), hypertension (67), and muscle atrophy (71). Recently, clinical trials have involved 315 the testing of TM5614 in patients with chronic myelogenous leukemia (72), metastatic melanoma 316 (73), non-small cell lung cancer (74), and angiosarcoma (75). Previous studies in humans carrying the SERPINE1<sup>TA700/+</sup> mutation provides compelling evidence that lifelong partial PAI-1 deficiency 317 318 is both well tolerated and protective. This human-based insight anchors the translational potential 319 of PAI-1 inhibition into effective clinical strategies. Together with ongoing clinical trials exploring 320 TM5614 in cancer, our findings demonstrate that TM5614 can also enhance organismal fitness 321 especially in delaying, or even reversing, cardiovascular aging.

## Methods

322

323

324

#### Sex as a biological variable

Our study examined both male and female humans and animal models. For humans and animals,

data were analyzed with sexes aggregated as well as separately.

#### **Human studies**

The population comprised individuals from an Old Order Amish population in Berne, IN, United States which harbors the c.699\_700dupTA frameshift mutation in *SERPINE1* that were previously described (25); this cross-sectional observational study included additional members (33 *SERPINE1*<sup>TA700/+</sup> and 33 *SERPINE1*<sup>+/+</sup>) that were not part of the original 2017 study. Participants were genotyped using polymerase chain reaction amplification specific for the c.699\_700dupTA frameshift. Study participants underwent PWV measurement by an experienced sonographer who was blind to participant genotype. PWV was measured noninvasively using the SphygmoCor® XCEL Vascular Biometric Monitor (AtCor Medical, Australia) according to the manufacturer's standard protocol. Participants were placed in a supine position, and measurements were obtained following a 10-minute rest period. Carotid-femoral PWV was calculated using applanation tonometry and oscillometric cuff data. To age and sex match the values from *SERPINE1*<sup>TA700/+</sup> participants, PWV values from the same age and sex *SERPINE1*<sup>+/+</sup> participants were randomly chosen to match *SERPINE1*<sup>TA700/+</sup> participants.

#### **Animal models**

#### Serpine1TA700/+ mice

This insertion was created a premature stop codon, resulting in a truncated mPAI-1 289 amino acid polypeptide, and concurrently abolish the BfmI (SfcI) restriction site at this location. The CRISPR-Cas9 reagents and repair template were electroporated into C57BL6/J zygotes at the Transgenic and Targeted Mutagenesis Laboratory of Northwestern University. Following electroporation, the zygotes were implanted into pseudopregnant female mice, and 20 F0 progeny were obtained. Genomic DNA was extracted from tail biopsies of the F0 mice and analyzed to confirm the presence of the desired mutation. The presence of the TA dinucleotide insertion was confirmed by Sanger sequencing in 3 out of the 20 F0 mice, which were found to be heterozygous. PCR amplification followed by SfcI digestion was employed as a genotyping strategy to screen for the mutation, as the TA insertion disrupted the SfcI recognition site at the end of exon 4. The resulting PCR amplicons from mutant alleles were resistant to SfcI digestion, while wild-type alleles were cleaved. These heterozygous F0 mice were used as the founders for subsequent breeding and maintenance on the C57BL6/J background to establish a colony for this work.

#### SERPINE1StabOE mice

PAI-1 transgenic mice were previously described (16), in which the murine preproendothelin-1 promoter was used to drive expression of a cDNA coding for the functionally stable variant of human PAI-1. These mice were maintained on the B6.D2 background.

#### Serpine1-GFP transgenic reporter mice

We previously reported the generation of a transgenic mouse line, 3kPAI-1-EGFP, that overexpresses enhanced green fluorescent protein under the control of the 3 kb proximal promoter of the human PAI-1 gene promoter (76). This line was maintained on the B6.D2 background and used for the experiment of 10 weeks L-NAME with concomitant TM5614 versus vehicle during the last six weeks of the experiment (Figure 6). This line has no gene mutation at the *Serpine1* locus; all mice in this line are *Serpine1*+/+.

#### L(ω)-nitro-L-arginine methyl ester (L-NAME) administration

L-NAME was used to inhibit eNOS and recapitulate vascular stiffening associated with increasing age. At 12 weeks of age, *Serpine1*<sup>TA700/+</sup> and *Serpine1*<sup>+/+</sup> mice were given L-NAME (ThermoFisher Scientific #H63666.14, Waltham, MA, USA) in drinking water (1mg/mL) for 8 weeks. Cardiovascular physiology (described later) was performed at baseline and after 8 weeks of L-NAME administration. For transcriptomics characterization, aortas were harvested after 8 weeks of L-NAME administration (described below).

#### TM5614 administration

L-NAME treatment in conjugation with PAI-1 inhibitor TM5614 (Renascience, Sendai, Japan) was used to capture the effects of pharmacological PAI-1 inhibition on vascular stiffening. 20-week-old *Serpine1*-GFP transgenic reporter mice underwent baseline cardiovascular characterization, received L-NAME (1mg/mL) for 4 weeks, and cardiovascular characterization was repeated. For the following 6 weeks, the mice continued 1mg/ml L-NAME; half received the oral PAI-1 inhibitor TM5614 (20 mg/kg/day) mixed in the standard chow, while the other half received control chow. Blood pressure and PWV measurements were performed a third time, and animals were euthanized for aorta collection.

### Cardiovascular physiology

All measurements described below were performed blind to genotype and/or treatment.

#### **Echocardiography**

Diastolic parameter E/e' were measured using the VEVO3100 ultrasound machine (FUJIFILM Visualsonics Corp., Toronto, ON, Canada). Mice were placed under anesthesia with isoflurane and positioned on a heating pad in a supine position, with anesthesia titrated to maintain heart rates above 500 for systolic and around 500 for diastolic measurements. Body temperature was controlled between 37 degrees Celsius using a heating lamp. A high-frequency ultrasound probe,

MX550D-25 to 55 MHz, (FUJIFILM Visualsonics Corp., Toronto, ON, Canada) was used to capture four-chamber and left ventricular parasternal long and short axis views of the heart. The data were subsequently analyzed for systolic and diastolic function measurements, as well as myocardial strain measurements, using VEVO Lab software (FUJIFILM Visualsonics Corp., Toronto, ON, Canada).

#### **Blood pressure**

Systolic blood pressures were measured using a non-invasive tail-cuff device (CODA® High Throughput System from Kent Scientific, Torrington, CT). Mice were placed in conical holders consciously for 15 minutes to acclimatize, and blood pressure measurements were taken over 40 cycles.

#### **Pulse wave velocity**

Pulse wave velocity (PWV) was measured in mice using the MX550D ultrasound probe on the VEVO3100 ultrasound machine (FUJIFILM Visualsonics Corp., Toronto, ON, Canada). Mice were placed under anesthesia with isoflurane and positioned in a supine position on a heating pad, with anesthesia titrated to maintain a heart rate above 500. Two pulse-wave Doppler images were obtained from the aorta, one proximal and one distal. B-Mode images were captured and analyzed using VEVO Lab software (FUJIFILM Visualsonics Corp., Toronto, ON, Canada), with the distance measured between the proximal and distal pulse waves, and the time from the QRS peak to the pulse wave in the aorta measured at these two locations. The software calculated PWV using the distance and time between the two set points.

#### Immunofluorescence

Aortas were harvested from mice and embedded OCT. Cryosectioning was used to obtain 10 micrometer-thick sections. The slides were permeabilized in 0.1% Triton-X 100 for 3 minutes, blocked in 0.2% BSA PBS for an hour, incubated with a polyclonal CCN1 antibody raised in rabbit

(Proteintech #26689-1-AP, Rosemont, IL, USA) at 4 degrees Celsius for 3 hours, washed 3 times with PBS, incubated with a goat anti rabbit IgG (H+L) secondary antibody conjugated with Alexa Fluor 488 (ThermoFisher Scientific #A-11008, Waltham, MA, USA), washed three times with PBS, dyed with Hoechst 33342 (ThermoFisher Scientific #H3570, Waltham, MA, USA), washed three times, and then mounted with Vectashield (Vector Laboratories #H-1000, Newark, CA, USA). Slides were kept in a fridge until imaging. Slides were then imaged using a Zeiss LSM980 microscope. Low-power images shown in Figure 4C and 4D were taken using a Plan Apochromat 10x/0.45 NA objective with the 488 laser at 1.2% power and identical contrast for all images. High-power images were taken using a Plan Apochromat 63x /1.3 NA high-resolution objective (Zeiss Group, Oberkochen, Baden-Württemberg, Germany). All images used in quantification (reported in Figure 4E) were taken using the 63x objective with the 488nm at 0.08% power and identical contrast for all images. The intensity of the fluorescence signal in stained slides was analyzed by a team member blind to genotype (S. S.) using ImageJ (NIH, USA). Briefly, images were converted to greyscale for the green and blue color channels and the intensity value for every pixel was determined by the function "analyze histogram" of ImageJ (NIH, USA). The aggregate intensity of all pixels was divided by the number of pixels that have a value over 100 that was determined experimentally based on the background fluorescence and the final value is presented as "mean intensity" for each slide.

#### **ELISA**

422

423

424

425

426

427

428

429

430

431

432

433

434

435

436

437

438

439

440

441

442

443

444

Circulating PAI-1 antigen levels in Serpine1<sup>TA700/+,</sup> Serpine1<sup>TA700/TA700</sup>, and Serpine1<sup>+/+</sup> mice were detected using a commercial ELISA kit for mouse total PAI-1 antigen (Innovative Research Inc #IMPAI1KTT, Novi, MI, USA) according to manufacturer's protocol.

#### **Transcriptomics**

#### Bulk RNA sequencing

Following L-NAME treatment, *Serpine1*<sup>TA700/+</sup> and *Serpine1*<sup>+/+</sup> mice were euthanized in a CO<sub>2</sub> chamber for 2 minutes. The aortas were isolated and underwent mild cleaning of the periaortic fat and excess tissue. RNA was isolated using the Qiagen RNeasy Mini Kit (Qiagen, Hilden, North Rhine-Westphalia, Germany) using the manufacturer protocol. RNA samples were sent to Novogene America Corp. Inc. (Novogene America Corp. Inc., Sacramento, CA, USA) for next generation mRNA sequencing. The aligned reads were analyzed using Python 3.9 (Python Software Foundation, Wilmington, DE, USA).

#### Single-Cell RNA sequencing

Single-cell analysis of L-NAME-treated *Serpine1*<sup>TA7000+</sup> and *Serpine1*<sup>+/+</sup> aortas was performed by adapting a previously described digestion protocol (43). A working enzyme solution was prepared on ice by combining Liberase TM (Roche #05401127001, Basel, Basel-Stadt, Switzerland) at 2 units/mL final concentration, Elastase (Worthington #LS002279, Columbus, OH, USA) at 2 units/mL final concentration, and DNase I at 60 units/mL (Roche #10104159001, Basel, Basel-Stadt, Switzerland) in HBSS with Ca<sup>2+</sup> and Mg<sup>2+</sup> (Gibco #14025092, Waltham, MA, USA).

After euthanization in a CO<sub>2</sub> chamber for 2 minutes, mice were perfused with 10 mL HBSS (Gibco #14025092, Waltham, MA, USA) via left ventricular puncture, and the aorta was harvested. The aortas underwent extensive cleaning of periaortic fat and excess tissue while submerged in MACS Separation Buffer (Miltenyi Biotec #130-091-221, Bergisch Gladbach, Rhineland, Germany). The aorta was split open and minced using iris scissors, transferred to 1mL of the enzyme solution described above, and incubated at 37°C for 45 minutes while shaking at 300 RPM. The reaction digestion reaction was stopped by adding 5 mL of 2% FBS (Gibco #A38401-01, Waltham, MA, USA) in HBSS (Gibco #14025092, Waltham, MA, USA). The cell suspension was passed through a 70-µm strainer into a 50 mL conical tube, and residual liquid was collected by centrifugation 300

× g for 10 minutes. Isolated cells were transferred into a microcentrifuge tube and centrifuged at 300 × g for 5 minutes. All but 100 μL of supernatant was removed and cells were resuspended in the remaining 100 μL volume. Cell viability was determined with Nexcelom Cellometer cell counter (Revvity, Waltham, MA, USA) and with the average of 86.3% viability with a range of 71% - 94%. Cell suspensions were submitted to the Integrative Genomics Core at the Robert H. Lurie Comprehensive Cancer Center of Northwestern University for partitioning and generation of transcriptomic libraries. Single-cell mRNA libraries were built using the Chromium Next GEM Single Cell 3' Library Construction V4 Kit. Libraries were sequenced using a high-output P4 flow cell (XLEAP chemistry) on an Illumina NextSeq 2000 sequencer (Illumina, Inc., San Diego, CA, USA), which generates up to 1.8 billion reads per run. Sequencing data were aligned to mouse reference using the Cell Ranger 3.0.2 pipeline (10X Genomics, Pleasanton, CA, USA). The data was analyzed using Python 3.9 (Python Software Foundation, Wilmington, DE, USA).

#### **Bioinformatics**

#### Single cell RNA sequencing preprocessing and analysis

scRNA-seq data from 32,354 cells were preprocessed to remove low-quality cells and doublets. Cells with >8% mitochondrial gene expression and outliers based on total counts, detected genes, and top 20 gene expression. Doublets were identified using a doubletdetection classifier python package (77) and removed. After filtering, data from 29,535 cells were used further processing. Data were then normalized and integrated using scanpy (1.10.0) and harmony (0.0.10) respectively.

Cell clustering was performed using the scanpy Leiden algorithm (resolution = 0.5) on adjusted principal components derived from harmony. Uniform Manifold Approximation and Projection (UMAP) was used to visualize the latent representation of the scRNA-seq data. Data were normalized, log-transformed, and visualized using scanpy UMAP. Differential gene expression

analysis identified marker genes, which were used for manual cell-type annotation. Uniform

Manifold Approximation and Projection (UMAP) was used to visualize the latent representation of the scRNA-seq data.

After integration, Wilcoxon rank-sum test (implemented in Scanpy) in rank gene groups function was used to compare gene groups and identify chondrocyte-like SMCs and ECM-Secretory SMCs. Using marker gene expression in clusters such as chondrocyte-associated markers (*Lgals3, Acan, Tnfrsf11b*) and fibroblast-associated markers (*Adamtsl1, Lama2, Fbln1, Vcan*), we assigned cell types. Gene expression was then used to distinguish chondrocyte-like SMCs and ECM-Secretory SMCs, respectively.

#### Differential gene expression and pathway enrichment analysis

Differential gene expression analysis was performed using the Wilcoxon rank-sum test on normalized counts to identify genes that were significantly upregulated or downregulated between genotypes. Significantly differentially expressed genes (p<0.05, adjusted for multiple comparisons) were classified as upregulated or downregulated based on their log fold change values. Violin plots were used to visualize differentially expressed genes based on log-normalized expression values. The Mann-Whitney U test was then applied to compare the expression distributions of the gene between the two genotypes. KEGG pathway enrichment analysis was then conducted using gseapy's enrichr function to determine biological pathways enriched among the upregulated and downregulated genes.

#### **RNA Velocity Analysis**

scRNA seq data were processed as described above. For RNA velocity analysis, we performed the following three steps: First, spliced and unspliced transcripts were quantified using Velocyto (version 0.17.17) to create gene expression count matrices. Second, we subsetted by genotypes and used scVelo (0.3.3) to log normalize count matrices, then a dynamical model was run to generate a UMAP representation with stream trajectories. Third, cellrank2 (version 2.0.7) was used to simulate random walks starting in the SMC cluster for both genotypes separately. Stream

trajectories in the *Serpine1*<sup>TA700/+</sup> genotype indicated a "backflow" from SMC cluster to the ECM-Secretory SMC cluster while this backflow was not present in wildtype mouse (Figure 6, A and B). To confirm this finding, cellrank2 random walks projection was performed with the SMC cluster set as starting point (Figure 6, C and D) and ECM-Secretory SMC cluster set as a starting point (Figure 6, E and F). Cellrank2 revealed that in *Serpine1*<sup>+/+</sup> mice, the SMCs transitioned towards Mature SMCs; in *Serpine1*<sup>TA700/+</sup> mice, SMCs transitioned towards ECM-Secretory SMCs and Fibroblasts (Figure 6, C-F) indicating altered terminal states of SMCs between the two genotypes.

#### Statistical analysis

The number of samples and the specific statistical parameters used for each experiment are included in the figure legends. To assess the effect of genotype on PWV, a multiple linear regression model was performed with PWV as the dependent variable and genotype, age, and sex and included as covariates. Two simple linear regressions were also performed on each genotype using PWV as the dependent variable and age as the independent variable in which analysis of covariance determined significance between the slope and elevation of the two separate regressions. Statistical testing was done using Prism 10.3 (GraphPad Software, San Diego, CA, USA). Threshold for statistical significance was set as p < 0.05.

#### Study approval

Northwestern University Institutional Review Board approved the study protocol, and all participants provided written informed consents. All animal studies were approved by the Northwestern University IACUC, and all characterizations followed the guidelines set by Northwestern University.

541	Data	Availa	bility
0 1 1	_ ~ ~	, ,, ,,,,	.~

- 542 All RNA sequencing data are available through Gene Expression Omnibus (GEO) accession
- 543 GSE297835 (Aorta sequencing). The Supporting Data Values file includes all individual data
- 544 points.

# **Author Contributions**

LDW and DEV designed experiments, supervised the research, and wrote the manuscript. A. Khoddam, A. Kalousdian, and LWD performed experiments, analyzed data, and wrote the manuscript. ME, SS, AD, EJL, BWZ, BD, BSC, CMC, and HA-V performed experiments and edited the manuscript. BZ and BB analyzed data. TM provided materials and edited the manuscript. A. Khoddam organized and wrote the majority of the manuscript, and for this reason he is listed first among to 2 co-first authors.

# Acknowledgments

This work is the result of NIH funding, in whole or in part, and is subject to the NIH Public Access Policy. Through acceptance of this federal funding, the NIH has been given a right to make the work publicly available in PubMed Central. This research was supported by NIH grants R35HL171553 (DEV) and R01AI170938 (CMC), and AHA Predoctoral Fellowship 25PRE1356859 (A. Khoddam). Transcriptomics and data analysis were performed by the Integrative Genomics branch of the Metabolomics Core Facility at Robert H. Lurie Comprehensive Cancer Center (generously supported by NCI CCSG P30 CA060553) of Northwestern University.

## References

- 1. Sillen M, Declerck PJ. Targeting PAI-1 in Cardiovascular Disease: Structural Insights Into PAI-
- 1 Functionality and Inhibition. *Front Cardiovasc Med*. 2020;7:622473.
- 2. Khoddam A, Vaughan D, Wilsbacher L. Role of plasminogen activator inhibitor-1 (PAI-1) in
- age-related cardiovascular pathophysiology. *J Cardiovasc Aging*. 2025;5(2).
- 565 https://doi.org/10.20517/jca.2024.38.
- 3. Kennelly PJ, et al. *Harper's illustrated biochemistry*. New York Chicago San Francisco Athens
- London Madrid Mexico City Milan New Delhi Singapore Sydney Toronto: McGraw Hill; 2023.
- 4. Kortlever RM, Higgins PJ, Bernards R. Plasminogen activator inhibitor-1 is a critical
- downstream target of p53 in the induction of replicative senescence. Nat Cell Biol.
- 570 2006;8(8):877–884.
- 571 5. Eren M, et al. Role of Plasminogen Activator Inhibitor-1 in Senescence and Aging. Semin
- 572 *Thromb Hemost*. 2014;40(06):645–651.
- 6. Vaughan DE, et al. Plasminogen Activator Inhibitor-1 Is a Marker and a Mediator of
- 574 Senescence. *ATVB*. 2017;37(8):1446–1452.
- 575 7. Eren M, et al. PAI-1-regulated extracellular proteolysis governs senescence and survival in
- 576 Klotho mice. Proc Natl Acad Sci USA. 2014;111(19):7090–7095.
- 577 8. Hamsten A, et al. Increased Plasma Levels of a Rapid Inhibitor of Tissue Plasminogen
- Activator in Young Survivors of Myocardial Infarction. *N Engl J Med*. 1985;313(25):1557–1563.
- 579 9. Thögersen AM, et al. High Plasminogen Activator Inhibitor and Tissue Plasminogen Activator
- Levels in Plasma Precede a First Acute Myocardial Infarction in Both Men and Women:

- 581 Evidence for the Fibrinolytic System as an Independent Primary Risk Factor. *Circulation*.
- 582 1998;98(21):2241–2247.
- 10. Lieb W, et al. Multimarker Approach to Evaluate Correlates of Vascular Stiffness: The
- Framingham Heart Study. Circulation. 2009;119(1):37–43.
- 585 11. Folsom AR, et al. Impact of weight loss on plasminogen activator inhibitor (PAI-1), factor VII,
- and other hemostatic factors in moderately overweight adults. *Arterioscler Thromb*.
- 587 1993;13(2):162–169.
- 12. Alessi M-C, Poggi M, Juhan-Vague I. Plasminogen activator inhibitor-1, adipose tissue and
- insulin resistance. *Current Opinion in Lipidology*. 2007;18(3):240–245.
- 13. Festa A, et al. Elevated Levels of Acute-Phase Proteins and Plasminogen Activator Inhibitor-
- 1 Predict the Development of Type 2 Diabetes. Diabetes. 2002;51(4):1131–1137.
- 592 14. Lu AT, et al. DNA methylation GrimAge strongly predicts lifespan and healthspan. Aging.
- 593 2019;11(2):303–327.
- 15. Kaikita K, et al. Potential Roles of Plasminogen Activator System in Coronary Vascular
- 595 Remodeling Induced by Long-term Nitric Oxide Synthase Inhibition. *Journal of Molecular and*
- 596 *Cellular Cardiology*. 2002;34(6):617–627.
- 597 16. Eren M, et al. Age-Dependent Spontaneous Coronary Arterial Thrombosis in Transgenic
- 598 Mice That Express a Stable Form of Human Plasminogen Activator Inhibitor-1. *Circulation*.
- 599 2002;106(4):491–496.
- 600 17. Diebold I, et al. The "PAI-1 paradox" in vascular remodeling. *Thromb Haemost*.
- 601 2008;100(6):984–991.

- 18. Garcia V, et al. Unbiased proteomics identifies plasminogen activator inhibitor-1 as a
- 603 negative regulator of endothelial nitric oxide synthase. *Proc Natl Acad Sci USA*.
- 604 2020;117(17):9497–9507.
- 19. Dai W, et al. Intracellular tPA-PAI-1 interaction determines VLDL assembly in hepatocytes.
- 606 Science. 2023;381(6661):eadh5207.
- 20. Khoddam A, Miyata T, Vaughan D. PAI-1 is a common driver of aging and diverse diseases.
- 608 Biomed J. 2025;100892.
- 609 21. Boe AE, et al. Plasminogen Activator Inhibitor-1 Antagonist TM5441 Attenuates N  $^{\omega}$  -Nitro- L
- -Arginine Methyl Ester-Induced Hypertension and Vascular Senescence. *Circulation*.
- 611 2013;128(21):2318–2324.
- 612 22. Hennan JK, et al. Evaluation of PAI-039 [{1-Benzyl-5-[4-(trifluoromethoxy)phenyl]-1 H-indol-
- 613 3-yl}(oxo)acetic Acid], a Novel Plasminogen Activator Inhibitor-1 Inhibitor, in a Canine Model of
- 614 Coronary Artery Thrombosis. The Journal of Pharmacology and Experimental Therapeutics.
- 615 2005;314(2):710–716.
- 23. Khoukaz HB, et al. Drug Targeting of Plasminogen Activator Inhibitor-1 Inhibits Metabolic
- Dysfunction and Atherosclerosis in a Murine Model of Metabolic Syndrome. ATVB.
- 618 2020;40(6):1479–1490.
- 619 24. Fay WP, et al. Human plasminogen activator inhibitor-1 (PAI-1) deficiency: characterization
- of a large kindred with a null mutation in the PAI-1 gene. *Blood*. 1997;90(1):204–208.
- 621 25. Khan SS, et al. A null mutation in *SERPINE1* protects against biological aging in humans.
- 622 Sci Adv. 2017;3(11):eaao1617.

- 623 26. North BJ, Sinclair DA. The intersection between aging and cardiovascular disease. *Circ*
- 624 Res. 2012;110(8):1097–1108.
- 625 27. Zhao D, et al. Impact of Aging on Cardiovascular Diseases: From Chronological Observation
- to Biological Insights: JACC Family Series. *JACC Asia*. 2024;4(5):345–358.
- 28. GBD 2021 Causes of Death Collaborators. Global burden of 288 causes of death and life
- expectancy decomposition in 204 countries and territories and 811 subnational locations, 1990-
- 629 2021: a systematic analysis for the Global Burden of Disease Study 2021. Lancet.
- 630 2024;403(10440):2100–2132.
- 631 29. Lyle AN, Raaz U. Killing Me Unsoftly: Causes and Mechanisms of Arterial Stiffness. ATVB.
- 632 2017;37(2). https://doi.org/10.1161/ATVBAHA.116.308563.
- 30. Hickson SS, et al. The Relationship of Age With Regional Aortic Stiffness and Diameter.
- 634 *JACC: Cardiovascular Imaging*. 2010;3(12):1247–1255.
- 635 31. Marshall AG, et al. Update on the Use of Pulse Wave Velocity to Measure Age-Related
- 636 Vascular Changes. *Curr Hypertens Rep.* 2024;26(3):131–140.
- 32. Wu S, et al. Aging, Arterial Stiffness, and Blood Pressure Association in Chinese Adults.
- 638 *Hypertension*. 2019;73(4):893–899.
- 639 33. Lu Y, et al. Trajectories of Age-Related Arterial Stiffness in Chinese Men and Women. J Am
- 640 *Coll Cardiol*. 2020;75(8):870–880.
- 34. Reference Values for Arterial Stiffness' Collaboration. Determinants of pulse wave velocity in
- healthy people and in the presence of cardiovascular risk factors: "establishing normal and
- 643 reference values." *Eur Heart J.* 2010;31(19):2338–2350.

- 35. Yingjie Ding, et al. Comprehensive human proteome profiles across a 50-year lifespan
- reveal aging trajectories and signatures. *Cell*. [published online ahead of print: 2025].
- 646 https://doi.org/10.1016/j.cell.2025.06.047.
- 36. Kolpakov V, Gordon D, Kulik TJ. Nitric Oxide–Generating Compounds Inhibit Total Protein
- and Collagen Synthesis in Cultured Vascular Smooth Muscle Cells. Circulation Research.
- 649 1995;76(2):305–309.
- 37. Yang Y-M, et al. eNOS uncoupling and endothelial dysfunction in aged vessels. *American*
- Journal of Physiology-Heart and Circulatory Physiology. 2009;297(5):H1829–H1836.
- 38. Vlachopoulos C, Aznaouridis K, Stefanadis C. Prediction of Cardiovascular Events and All-
- 653 Cause Mortality With Arterial Stiffness. *Journal of the American College of Cardiology*.
- 654 2010;55(13):1318–1327.
- 39. Küng CF, et al. L-NAME Hypertension Alters Endothelial and Smooth Muscle Function in
- 656 Rat Aorta: Prevention by Trandolapril and Verapamil. *Hypertension*. 1995;26(5):744–751.
- 40. De Moudt S, et al. Aortic Stiffness in L-NAME Treated C57Bl/6 Mice Displays a Shift From
- 658 Early Endothelial Dysfunction to Late-Term Vascular Smooth Muscle Cell Dysfunction. Front
- 659 *Physiol.* 2022;13:874015.
- 41. Paulis L, et al. Direct Angiotensin II Type 2 Receptor Stimulation in  $N^{\omega}$  -Nitro- L -Arginine-
- Methyl Ester-Induced Hypertension: The Effect on Pulse Wave Velocity and Aortic Remodeling.
- 662 Hypertension. 2012;59(2):485–492.
- 42. Carramolino L, et al. Cholesterol lowering depletes atherosclerotic lesions of smooth muscle
- cell-derived fibromyocytes and chondromyocytes. *Nat Cardiovasc Res*. 2024;3(2):203–220.

- 665 43. Cheng P, et al. Smad3 regulates smooth muscle cell fate and mediates adverse remodeling
- and calcification of the atherosclerotic plaque. *Nat Cardiovasc Res.* 2022;1(4):322–333.
- 667 44. Younesi FS, et al. Fibroblast and myofibroblast activation in normal tissue repair and
- 668 fibrosis. Nat Rev Mol Cell Biol. 2024;25(8):617–638.
- 45. Bassat E, Tzahor E. How Can Young Extracellular Matrix Promote Cardiac Regeneration?
- 670 Versi-Can! *Circulation*. 2024;149(13):1016–1018.
- 46. Feng J, et al. Versican Promotes Cardiomyocyte Proliferation and Cardiac Repair.
- 672 *Circulation*. 2024;149(13):1004–1015.
- 673 47. Madeo F, et al. Essential role for autophagy in life span extension. *J Clin Invest*.
- 674 2015;125(1):85–93.
- 48. Kops GJPL, et al. Forkhead transcription factor FOXO3a protects quiescent cells from
- 676 oxidative stress. *Nature*. 2002;419(6904):316–321.
- 49. Liu L, et al. *LRP1* Repression by SNAIL Results in ECM Remodeling in Genetic Risk for
- Vascular Diseases. Circulation Research. 2024;135(11):1084–1097.
- 50. Jun J-I, Lau LF. The matricellular protein CCN1 induces fibroblast senescence and restricts
- fibrosis in cutaneous wound healing. *Nat Cell Biol.* 2010;12(7):676–685.
- 51. Jun J-I, Lau LF. CCN2 induces cellular senescence in fibroblasts. *J Cell Commun Signal*.
- 682 2017;11(1):15–23.
- 52. Won JH, Choi JS, Jun J-I. CCN1 interacts with integrins to regulate intestinal stem cell
- proliferation and differentiation. *Nat Commun.* 2022;13(1):3117.

- 53. Abdellatif M, et al. Hallmarks of cardiovascular ageing. Nat Rev Cardiol. 2023;20(11):754–
- 686 777.
- 54. La Manno G, et al. RNA velocity of single cells. *Nature*. 2018;560(7719):494–498.
- 55. Lange M, et al. CellRank for directed single-cell fate mapping. *Nat Methods*.
- 689 2022;19(2):159-170.
- 56. Flevaris P, et al. Plasminogen Activator Inhibitor Type I Controls Cardiomyocyte
- Transforming Growth Factor-β and Cardiac Fibrosis. *Circulation*. 2017;136(7):664–679.
- 57. Khan SS, et al. Identification of Cardiac Fibrosis in Young Adults With a Homozygous
- 693 Frameshift Variant in SERPINE1. JAMA Cardiol. 2021;6(7):841.
- 58. Gupta KK, et al. Plasminogen Activator Inhibitor-1 Protects Mice Against Cardiac Fibrosis by
- 695 Inhibiting Urokinase-type Plasminogen Activator-mediated Plasminogen Activation. Sci Rep.
- 696 2017;7(1):365.
- 697 59. Ghosh AK, Vaughan DE. PAI-1 in tissue fibrosis. *J Cell Physiol*. 2012;227(2):493–507.
- 698 60. Obesity and overweight [Internet]. 2024. https://www.who.int/news-room/fact-
- 699 sheets/detail/obesity-and-overweight.
- 700 61. Asselbergs FW, et al. The gender-specific role of polymorphisms from the fibrinolytic, renin-
- angiotensin, and bradykinin systems in determining plasma t-PA and PAI-1 levels. *Thromb*
- 702 *Haemost*. 2006;96(4):471–477.
- 703 62. Blokland KEC, et al. Regulation of cellular senescence by extracellular matrix during chronic
- 704 fibrotic diseases. *Clin Sci (Lond)*. 2020;134(20):2681–2706.

- 705 63. Lau LF. CCN1 and CCN2: blood brothers in angiogenic action. *J Cell Commun Signal*.
- 706 2012;6(3):121–123.
- 707 64. Hsu P-L, et al. Shear-Induced CCN1 Promotes Atheroprone Endothelial Phenotypes and
- 708 Atherosclerosis. Circulation. 2019;139(25):2877–2891.
- 709 65. Puy C, et al. Endothelial PAI-1 (Plasminogen Activator Inhibitor-1) Blocks the Intrinsic
- 710 Pathway of Coagulation, Inducing the Clearance and Degradation of FXIa (Activated Factor XI).
- 711 *ATVB*. 2019;39(7):1390–1401.
- 712 66. Handt S, et al. Plasminogen activator inhibitor-1 secretion of endothelial cells increases
- 713 fibrinolytic resistance of an in vitro fibrin clot: evidence for a key role of endothelial cells in
- 714 thrombolytic resistance. *Blood*. 1996;87(10):4204–4213.
- 715 67. Yunes-Leites PS, et al. Phosphatase-independent activity of smooth-muscle calcineurin
- orchestrates a gene expression program leading to hypertension. *PLoS Biol.*
- 717 2025;23(5):e3003163.
- 718 68. Oliveira J, et al. LAMA2 Muscular Dystrophy. In: Adam MP, et al., eds. *GeneReviews*®.
- 719 Seattle (WA): University of Washington, Seattle; 1993.
- 720 69. Levine JA, et al. Role of PAI-1 in hepatic steatosis and dyslipidemia. Sci Rep.
- 721 2021;11(1):430.
- 722 70. Levine J, et al. OR22-6 Reversal Of Diet Induced Metabolic Syndrome In Mice With An
- 723 Orally Active Small Molecule Inhibitor Of PAI-1. *Journal of the Endocrine Society*.
- 724 2019;3(Supplement 1):OR22-6.
- 725 71. Aihemaiti A, et al. A novel PAI-1 inhibitor prevents ageing-related muscle fiber atrophy.
- 726 Biochemical and Biophysical Research Communications. 2021;534:849–856.

- 727 72. Takahashi N, et al. Deep molecular response in patients with chronic phase chronic myeloid 728 leukemia treated with the plasminogen activator inhibitor-1 inhibitor TM5614 combined with a 729 tyrosine kinase inhibitor. Cancer Medicine. 2023;12(4):4250–4258. 730 73. Fujimura T, et al. A phase II multicentre study of plasminogen activator inhibitor-1 inhibitor 731 (TM5614) plus nivolumab for treating anti-programmed cell death 1 antibody-refractory 732 malignant melanoma: TM5614-MM trial. British Journal of Dermatology. 2024;191(5):691–697. 733 74. Masuda T, et al. EP.11D.02 An Investigator-Initiated Phase II Study of Combination 734 Treatment of Nivolumab and TM5614, A PAI-1 Inhibitor for Previously Treated NSCLC. Journal 735 of Thoracic Oncology. 2024;19(10):S614. 736 75. Fujimura T, et al. Efficacy and safety of TM5614 in combination with paclitaxel in the 737 treatment of paclitaxel-resistant cutaneous angiosarcoma: Phase II study protocol. Experimental 738 Dermatology. 2024;33(1):e14976. 739 76. Eren M, et al. Tissue- and agonist-specific regulation of human and murine plasminogen 740 activator inhibitor-1 promoters in transgenic mice. *J Thromb Haemost*. 2003;1(11):2389–2396.
- 741 77. Adam Gayoso, Jonathan Shor. JonathanShor/DoubletDetection: doubletdetection
- 742 v4.3.0.post1. 2025. https://doi.org/10.5281/ZENODO.2678041.

# 744 Figures

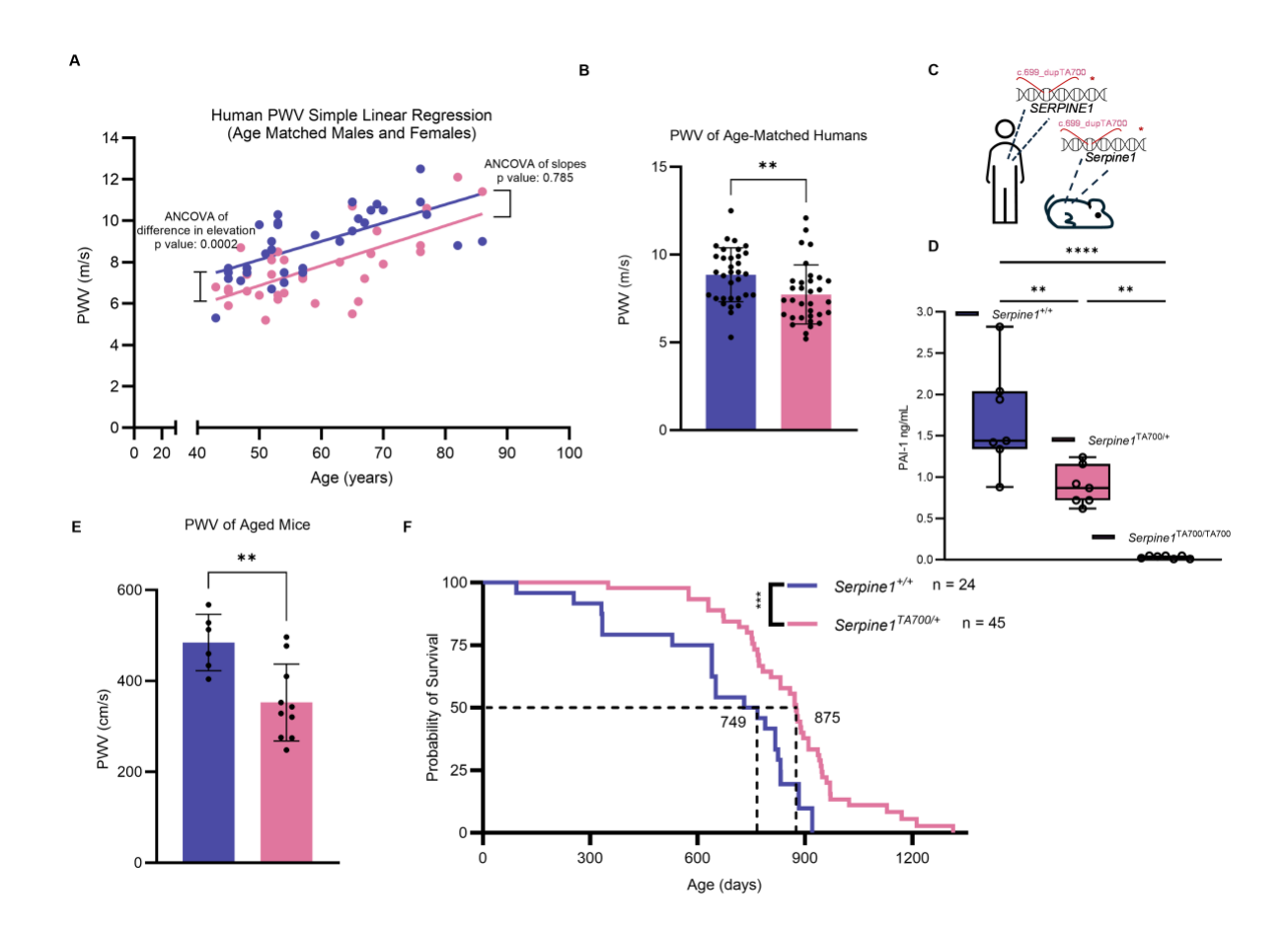


**Figure 1.** *SERPINE1* haploinsufficiency is associated with improved vascular function in humans and longer lifespan in mice. (**A**) Scatterplot of PWV as a function of age in age and sex matched *SERPINE1*<sup>TA700/+</sup> (n= 33, 11 males and 22 females) individuals. Simple linear regression was used to assess PWV as a function of age. (**B**) Aggregated human PWV values. (**C**) Schematic of the mouse line harboring a dinucleotide duplication in the mouse gene *Serpine1*. (**D**) Serum PAI-1 levels measured by detecting PAI-1 antigen using ELISA (n=7 per genotype). (**E**) Comparison of Aged (600 days and older) *Serpine1*<sup>TA700/+</sup> (n= 10; 6 males and 4 females). (**F**) Overall survival of *Serpine1*<sup>TA700/+</sup> and control *Serpine1*<sup>T/+</sup> mice (9 male and 15 female *Serpine1*<sup>+/+</sup>; 27 male and 18 female *Serpine1*<sup>TA700/+</sup>). To determine significance, analysis of covariance was used in (**A**), two-tailed unpaired t-test was used in (**B**) and (**E**), ordinary one-way ANOVA was used in (**D**), and Log Rank test was used in (**F**). \*\*, p < 0.01; \*\*\*\*, p < 0.001; \*\*\*\*\*, p < 0.001; \*\*\*\*\*, p < 0.0001.

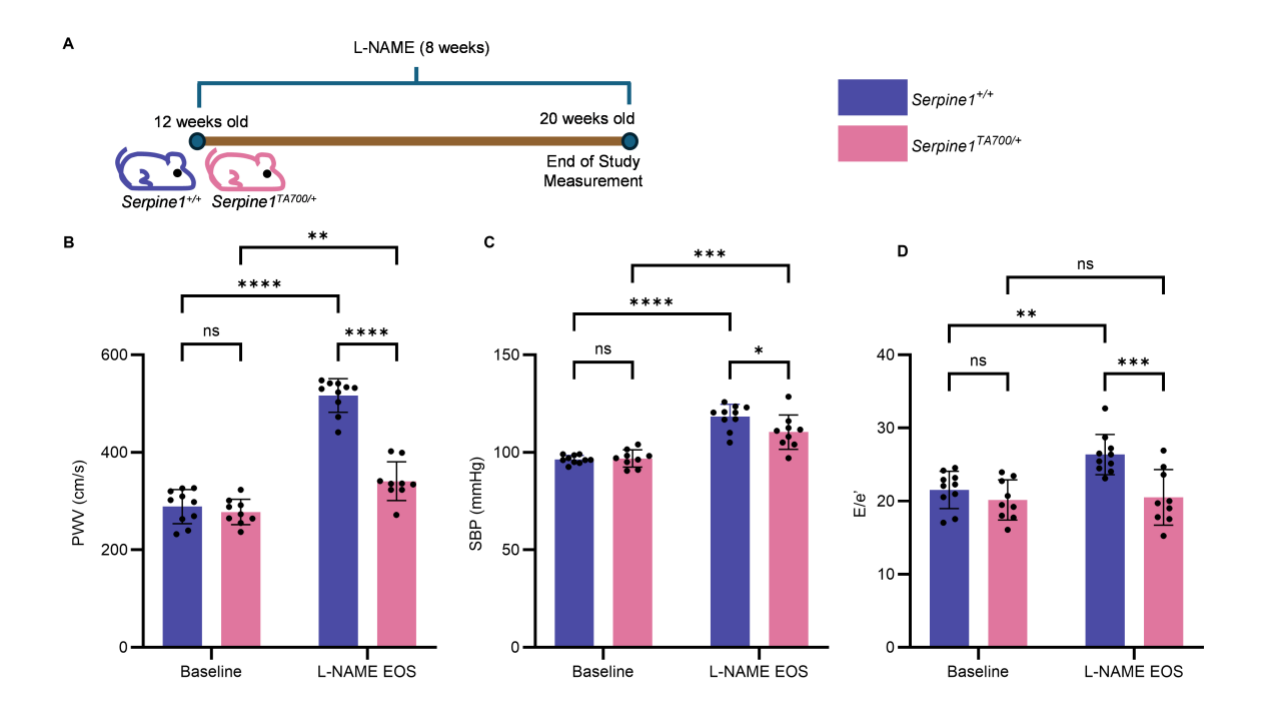


Figure 2. Serpine 1<sup>TA700/+</sup> Mice Exhibit Protection Against Cardiovascular Pathophysiology Associated with L-NAME. (A) Schematic of the study: Serpine 1<sup>+/+</sup> n=10 with 7 males and 3 females; Serpine 1<sup>TA700/+</sup> n=9 with 6 males and 3 females. (B) PWV (C) SBP, and (D) E/e' of Serpine 1<sup>TA700/+</sup> mice compared to littermate controls at baseline at End of Study (EOS). To determine significant interactions between variables, two-way ANOVA was used in (B-D). ns = not significant; \*, p < 0.05; \*\*, p< 0.01; \*\*\*p < 0.001; \*\*\*\*\*, p < 0.0001.

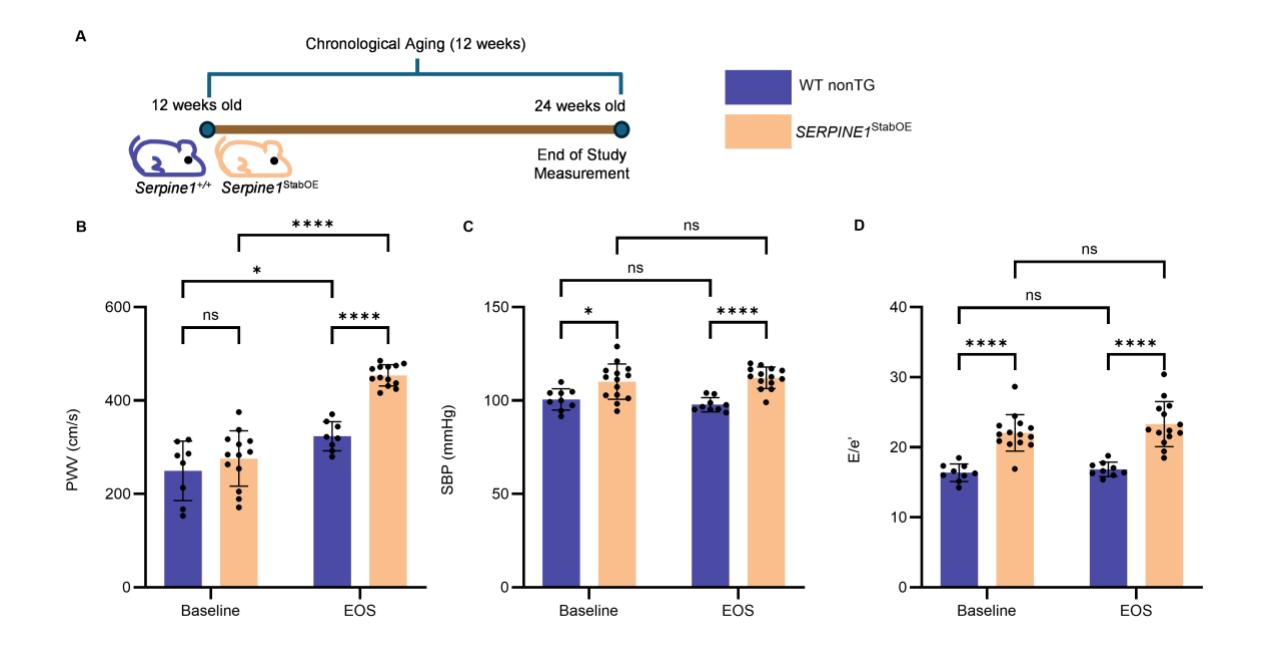


Figure 3. SERPINE1<sup>StabOE</sup> Mice Exhibit Elevated Cardiovascular Pathophysiology. (A) Schematic of the study: WT nonTG n=9 with 5 males and 4 females; SERPINE1<sup>StabOE</sup> n=14 with 5 males and 9 females used for SBP measurements and SERPINE1<sup>StabOE</sup> n=13 with 4 males and 9 females used for E/e' and PWV. (B) PWV (C) SBP, and (D) E/e' of SERPINE1<sup>StabOE</sup> mice compared to littermate controls at 12 weeks of age (Baseline) at 24 weeks of age (End of Study or EOS). To determine significant interactions between variables, two-way ANOVA was used in (B-D). \*, p < 0.05; \*\*\*\*\*, p < 0.0001.

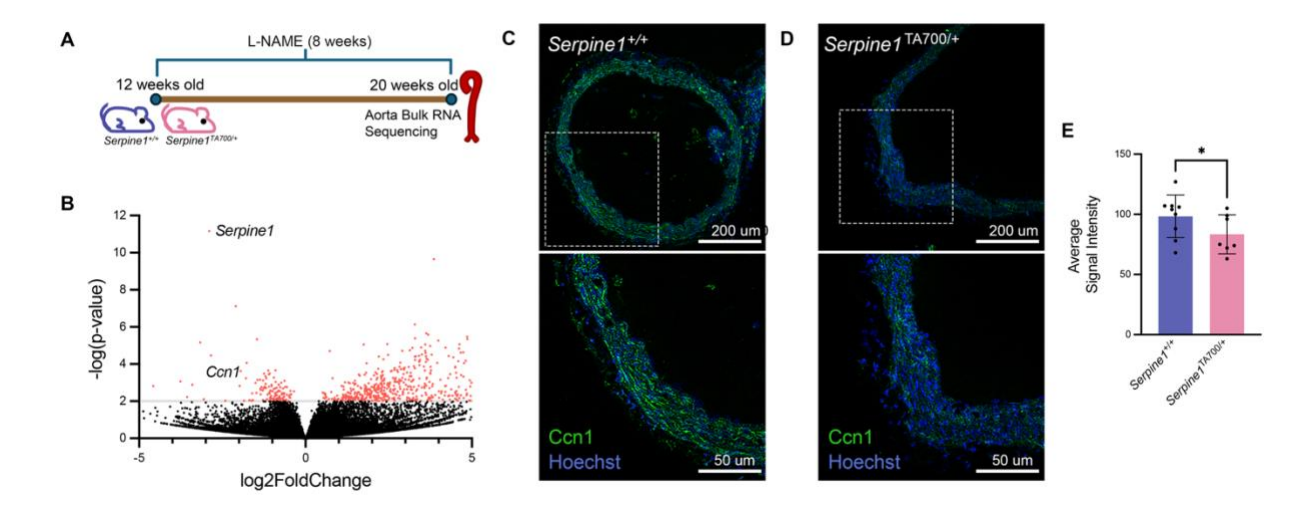
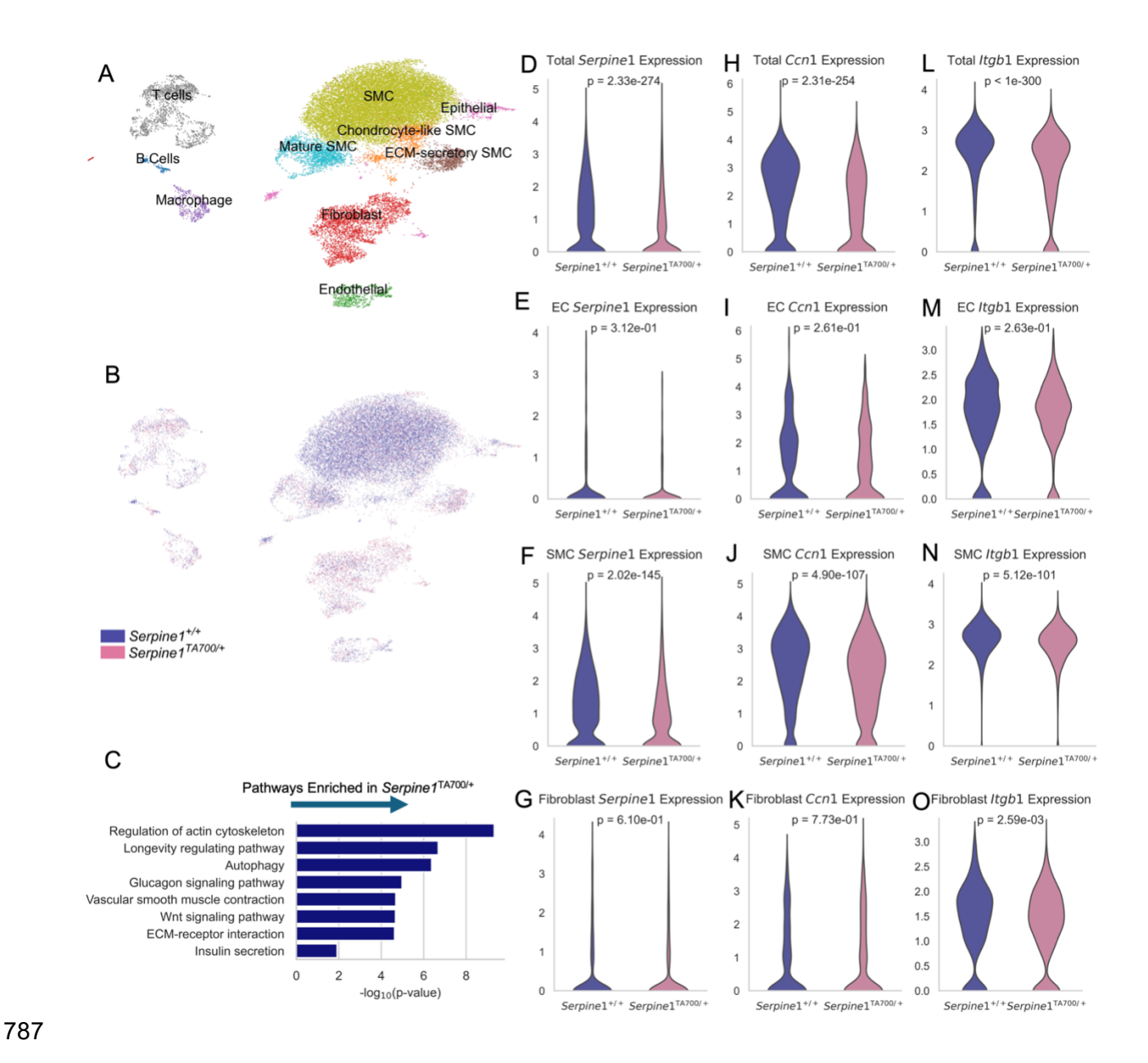


Figure 4. *Ccn1* Transcript and Protein Expression Is Altered in aorta from *Serpine1*<sup>TA700/+</sup> mice. (A) Schematic of the study. (B) Differentially Expressed Genes of *Serpine1*<sup>TA700/+</sup> (3 males and 3 females) compared to littermate controls (3 males and 3 females) using bulk RNA sequencing of aortas. (C and D) Confocal images of immunofluorescent signals of CCN1 (green) and nuclei (blue) in aortas from *Serpine1*<sup>+/+</sup> (C) and *Serpine1*<sup>TA700/+</sup> (D) mice. (E) Quantification of aorta CCN1 signal intensity from 9 *Serpine1*<sup>+/+</sup> (4 males and 5 females) and 7 *Serpine1*<sup>TA700/+</sup> (4 males and 3 females) mice. To determine significance, DESeq2 was used in (B) and a one-tail Mann-Whitney U-test was used in (E). \*p < 0.05.



**Figure 5.** scRNA-seq of aortas from *Serpine1*<sup>TA700/+</sup> and *Serpine1*<sup>+/+</sup> mice. (A) UMAP plot showing the clustering of all cells sequenced from aortas of 4 *Serpine1*<sup>TA700/+</sup> (2 males and 2 females) and 6 *Serpine1*<sup>+/+</sup> mice (3 males and 3 females). (B) UMAP plot showing composition of sequenced cells from each genotype. (C) Pathway enrichment analysis was done on genes overrepresented in total *Serpine1*<sup>TA700/+</sup> and *Serpine1*<sup>+/+</sup>cells using KEGG. (D-O) Violin plots showing log-normalized gene expression of *Serpine1*, *Ccn1*, and *Itgb1* in total, endothelial cells, SMCs, and fibroblasts in the two genotypes. Mann-Whitney U-test was used to test for significance in differential expression of genes in (D-O).

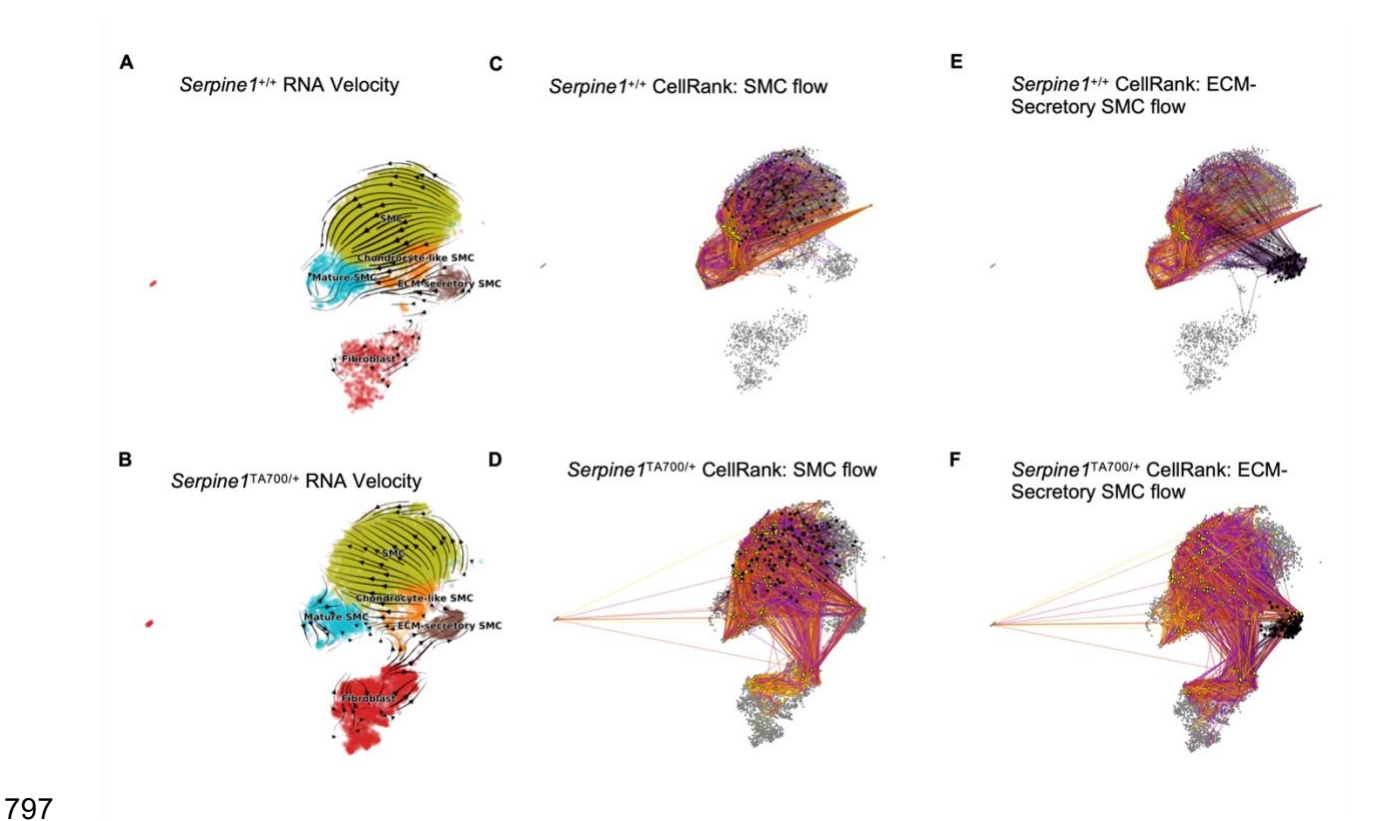
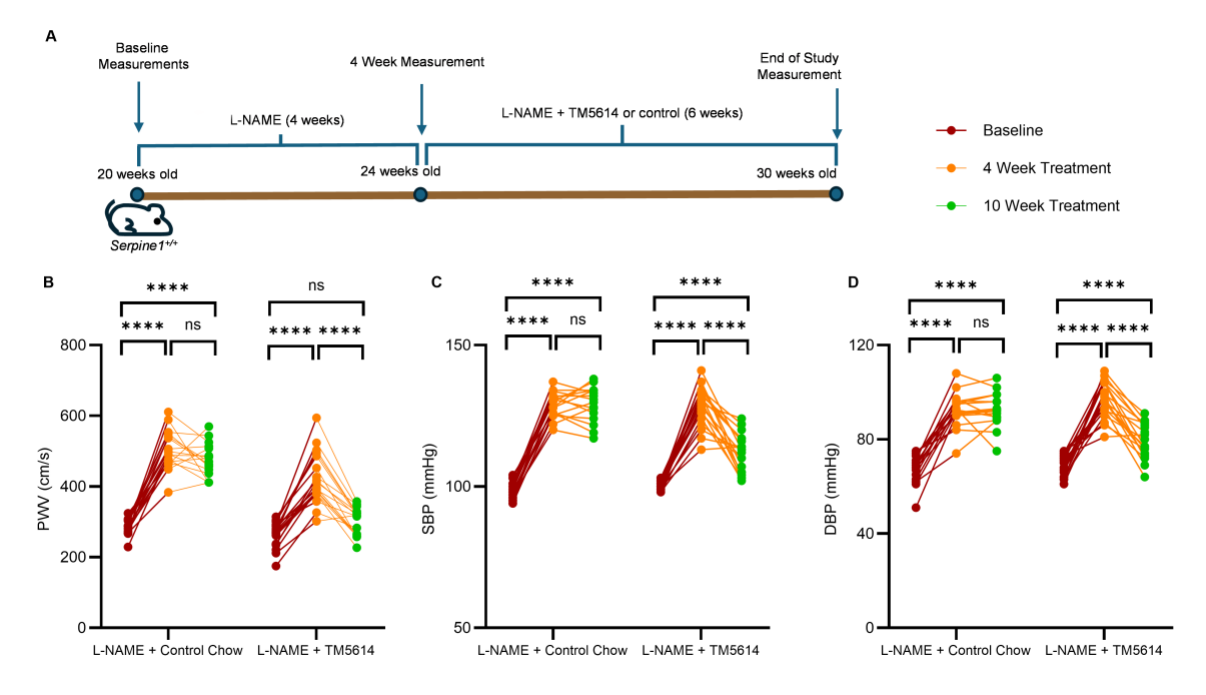


Figure 6. RNA velocity and CellRank analyses reveal altered cell state dynamics in Serpine1<sup>TA700/+</sup> aortas. (A–B) Steady-state RNA velocity stream plots showing transcriptional dynamics within fibroblast and smooth muscle cell (SMC) lineages in Serpine1<sup>+/+</sup> (A) and Serpine1<sup>TA700/+</sup> (B) aortas. Arrows indicate the inferred direction of cell state transitions, revealing more restricted trajectories in controls and greater plasticity in Serpine1<sup>TA700/+</sup> mice. (C–F) CellRank fate mapping visualizations indicating transitions from SMCs (C and D) and ECM-Secretory SMCs (E and F). Initial states are shown in black, terminal states in yellow, and directed edges represent cell fate probabilities from each starting point. Darker arrows represent higher transition probabilities in Serpine1<sup>+/+</sup> (C and E) and Serpine1<sup>TA700/+</sup> (D and F) aortas.



**Figure 7. TM5614 Administration Reverses the L-NAME-Induced Increase in BP and PWV.**(A) Schematic of the study. (B) PWV, (C) SBP, and (D) DBP of mice receiving control chow (left) or TM5614 (right) at baseline, 4 weeks, and end of study. Mice receiving Control Chow: 7 males and 9 females; mice receiving TM5614: 9 males and 10 females. An ordinary one-way ANOVA with Tukey correction for multiple comparisons was used to determine significance in (B-D). \*\*\*\*, p < 0.0001.

**Table 1** 816

Variable	Parameter Estimate	Standard Error	P value	95% Confidence Interval
Genotype[SERPINE1TA700/+]	-1.182	0.803	0.0002	(-1.784, -0.580)
Sex[Male]	0.422	0.322	0.148	(-0.222, 1.067)
Age	0.090	0.013	>0.0001	(0.064, 0.117)

**Table 1.** *SERPINE1* haploinsufficiency is associated with improved vascular function in humans. Multiple linear regression was used to assess the effects of genotype, sex, and age on pulse wave velocity (PWV). Table presents PWV parameter estimates (in meters/second), standard error, p value, and the 95% confidence interval associated with each variable.